EURASIP Journal on Applied Signal Processing 2005:5, 730–742

Joint Impact of Frequency Synchronization Errors and Intermodulation Distortion on the Performance of Multicarrier DS-CDMA Systems

Luca Rugini
Dipartimento di Ingegneria Elettronica e dell'Informazione (DIEI), Università degli Studi di Perugia, Via G. Duranti 93, 06125 Perugia, Italy
Email: rugini@diei.unipg.it

Paolo Banelli
Dipartimento di Ingegneria Elettronica e dell'Informazione (DIEI), Università degli Studi di Perugia, Via G. Duranti 93, 06125 Perugia, Italy
Email: banelli@diei.unipg.it

Received 5 August 2003; Revised 19 January 2004

The performance of multicarrier systems is highly impaired by intercarrier interference (ICI) due to frequency synchronization errors at the receiver and by intermodulation distortion (IMD) introduced by a nonlinear amplifier (NLA) at the transmitter. In this paper, we evaluate the bit-error rate (BER) of multicarrier direct-sequence code-division multiple-access (MC-DS-CDMA) downlink systems subject to these impairments in frequency-selective Rayleigh fading channels, assuming quadrature amplitude modulation (QAM). The analytical findings allow to establish the sensitivity of MC-DS-CDMA systems to carrier frequency offset (CFO) and NLA distortions, to identify the maximum CFO that is tolerable at the receiver side in different scenarios, and to find out the optimum value of the NLA output power backoff for a given CFO. Simulation results show that the approximated analysis is quite accurate in several conditions.

Keywords and phrases: multicarrier DS-CDMA, carrier frequency offset, intermodulation distortion, Rayleigh fading.

1. INTRODUCTION

In the last years, several multicarrier code-division multiple-access (MC-CDMA) schemes [1] have been proposed by combining orthogonal frequency-division multiplexing (OFDM) and direct-sequence code-division multiple-access (DS-CDMA), with the goal of incorporating the advantages of both techniques. Specifically, the low-complexity equalization of cyclic prefixed OFDM systems and the multiple-access interference (MAI) mitigation capabilities offered by DS-CDMA systems make MC-CDMA techniques attractive for future mobile broadband communications [2].

Differently from single-carrier systems, one of the main problems of multicarrier schemes is the high sensitivity to frequency synchronization errors [3]. Indeed, the carrier frequency offset (CFO), which models the frequency mismatch between the transmitter and receiver oscillators, generates intercarrier interference (ICI), thereby destroying the frequency-domain orthogonality of the transmitted data.

The presence of a nonlinear amplifier (NLA) at the transmitter, which introduces both intermodulation distortion (IMD) and out-of-band interference, is another relevant source of impairment in multicarrier systems. Indeed, multicarrier signals are characterized by a high peak-to-average power ratio (PAPR) [4], and hence they are significantly distorted when, in order to improve the power efficiency, the NLA working point is chosen close to the saturation point.

Obviously, the typical impairments of multicarrier systems add to the sources of degradation that are generally present also in other multiple-access schemes, such as the MAI associated with multiple users in nonorthogonal systems [5], and the intersymbol interference (ISI) introduced by the signal propagation over multipath channels. As a consequence, the degradation introduced by CFO and NLA, as well as MAI and multipath, should be taken into account when evaluating the performance of multicarrier systems.

Specifically, this paper deals with the effects of the mentioned impairments on the bit-error rate (BER) performance. The particular multicarrier scheme herein considered

is commonly identified as multicarrier DS-CDMA (MC-DS-CDMA) [1], where multiple users are discriminated by spreading in the time domain. Moreover, in this paper, we focus on the performance at the mobile end (i.e., downlink), assuming that the receiver is equipped with a bank of single-tap equalizers followed by a despreader.

Previous works about MC-DS-CDMA performance considered the presence of either frequency synchronization errors or nonlinear distortions. Indeed, Steendam and Moeneclaey evaluated the signal-to-noise ratio (SNR) degradation produced by the CFO in additive white Gaussian noise (AWGN) for MC-DS-CDMA downlink systems [6]; however, they did not consider the NLA at the transmitter. In addition, Jong and Stark analyzed the effects of multipath and nonlinearities on the BER performance of a multicarrier spread-spectrum system, which basically is an MC-DS-CDMA scheme with one active user [7]. However, they assumed perfect frequency synchronization at the receiver side.

The purpose of our work is to extend the results of [6, 7] in order to jointly take into account CFO, nonlinear distortions, and MAI, in multipath fading channels. Our two-step approach to obtain the BER is quite standard. The first step relies on the Gaussian approximation of the interferences, which allows us to evaluate the BER conditioned on a given channel realization. The second step consists in averaging the conditional BER over the channel statistic, which is assumed to be Rayleigh.

The paper is structured as follows. In Section 2, we introduce an MC-DS-CDMA system model where linear signal processing operations (either in the time domain or in the frequency domain) are simply represented by matrix multiplications. Section 3 is dedicated to the BER evaluation in frequency-flat fading channels, assuming quadrature amplitude modulation (QAM). In Section 4, the BER evaluation for flat-fading channels is extended to frequency-selective scenarios characterized by Rayleigh fading. In Section 5, we check the accuracy of the analytical findings by comparing theoretical and simulated results. Finally, in Section 6, some concluding remarks are drawn.

2. SYSTEM MODEL

Firstly, we introduce some basic notations. We use lower (upper) bold face letters to denote column vectors (matrices), superscripts $*$, T, and H to represent complex conjugate, transpose, and Hermitian operators, respectively. We reserve $E\{\cdot\}$ to represent the statistical expectation, and $\lfloor x \rfloor$ to denote the greatest integer smaller than or equal to x. The Q-function is defined as $Q(x) = (2\pi)^{-1/2} \int_x^{+\infty} e^{-\nu^2/2} d\nu$, $\mathbf{0}_{M\times N}$ is the $M \times N$ all-zero matrix, and $\mathbf{I}_N$ is the $N \times N$ identity matrix. We define $[\mathbf{A}]_{m,n}$ as the (m,n)th entry of the matrix $\mathbf{A}$, $[\mathbf{a}]_n$ as the nth entry of the column vector $\mathbf{a}$, $(a)_{\mathrm{mod}\, N}$ as the remainder after division of a by N, and $\mathrm{diag}(\mathbf{a})$ as the diagonal matrix with (n,n)th entry equal to $[\mathbf{a}]_n$.

We consider the downlink of an MC-DS-CDMA system with N subcarriers, spaced by $\Delta_f = 1/T$, and with K active users. Hence, assuming rectangular pulse shaping, the chip duration is equal to T. The base station transmits N symbols of each user in parallel, one for each subcarrier, by spreading each symbol in the time domain employing a user-dependent spreading code. The spreading code of the kth user, which is the same for all the subcarriers, is denoted by $\mathbf{c}_k = [c_{k,0} \ \cdots \ c_{k,G-1}]^T$, where G is the processing gain. Assuming $|c_{k,g}| = G^{-1/2}$, the vector $\mathbf{c}_k$ has unit norm. As in conventional OFDM systems, the time-domain samples are obtained by N-dimensional IFFT of the data on the N subcarriers, and a cyclic prefix of duration $\tau_{\mathrm{CP}} = LT/N$ is attached to the IFFT output block in order to avoid channel-induced interference between successive blocks. Consequently, the symbol rate of each user is equal to $N/(1 + L/N)GT$.

By defining the $N \times N$ unitary FFT matrix $\mathbf{F}$ as $[\mathbf{F}]_{m,n} = N^{-1/2} \exp(-j2\pi(m-1)(n-1)/N)$, and the $(N+L)\times N$ cyclic prefix insertion matrix as $\mathbf{T}_{\mathrm{CP}} = [\mathbf{I}_{\mathrm{CP}}^T \ \ \mathbf{I}_N^T]^T$, where $\mathbf{I}_{\mathrm{CP}}$ contains the last L rows of the identity matrix $\mathbf{I}_N$, the transmitted block, at the input of the NLA, can be expressed by [8]

$$\mathbf{u}_{\mathrm{IN}}[lG + g] = \mathbf{T}_{\mathrm{CP}}\mathbf{F}^H\mathbf{S}[l]\mathbf{c}[g], \tag{1}$$

where $\mathbf{u}_{\mathrm{IN}}[lG + g]$ is a vector of dimension $P = N + L$, $\mathbf{S}[l]$ is the $N \times K$ matrix containing the data symbols, with $s_{n,k}[l] = [\mathbf{S}[l]]_{n,k}$ the lth symbol of the kth user on the nth subcarrier, and $\mathbf{c}[g] = [c_{1,g} \ \cdots \ c_{K,g}]^T$ is the vector that contains the gth chip of the spreading codes of all the K users. The data symbols $\{s_{n,k}[l]\}$, drawn from an M-ary square QAM constellation, are assumed to be independent and identically distributed (i.i.d.) with power σ_S^2. Although in many cases we are dealing with continuous-time signals (i.e., at the NLA input and output, at the receiver input, etc.), throughout the paper we consider the equivalent discrete-time signals, to simplify the notation.

In this paper, we model the NLA as a memoryless device characterized by its AM/AM and AM/PM curves. After incorporating both the chip index g and the symbol index l into a single index $i = lG + g$, by the Bussgang theorem [9], the transmitted block, at the output of the NLA, can be expressed as [10, 11]

$$\mathbf{u}_{\mathrm{OUT}}[i] = \alpha\mathbf{u}_{\mathrm{IN}}[i] + \bar{\mathbf{v}}_{\mathrm{IMD}}[i], \tag{2}$$

where α represents the average linear amplification gain, and $\bar{\mathbf{v}}_{\mathrm{IMD}}[i]$ is the intermodulation distortion (IMD), uncorrelated with the linear part $\alpha\mathbf{u}_{\mathrm{IN}}[i]$. The validity of (2), based on a Gaussian distribution of $\mathbf{u}_{\mathrm{IN}}[i]$ in (1), is justified by the high number of subcarriers usually employed in multicarrier systems (e.g., $N > 32$) [11]. In this case, the average linear amplification gain can be evaluated as $\alpha = R_{u_{\mathrm{OUT}}u_{\mathrm{IN}}}(0)/R_{u_{\mathrm{IN}}u_{\mathrm{IN}}}(0)$, where $R_{u_{\mathrm{OUT}}u_{\mathrm{IN}}}(\tau)$ is the continuous-time cross-correlation between the NLA output and input, and $R_{u_{\mathrm{IN}}u_{\mathrm{IN}}}(\tau)$ is the continuous-time autocorrelation

function of the NLA input. Moreover, the elements of

$$\mathbf{R}_{\tilde{\mathbf{v}}}(g,g') = E\{\tilde{\mathbf{v}}_{\mathrm{IMD}}[lG+g]\tilde{\mathbf{v}}_{\mathrm{IMD}}[lG+g']^H\} \tag{3}$$

can be predicted in advance by exploiting the knowledge of the continuous-time autocorrelation function $R_{u_{\mathrm{OUT}}u_{\mathrm{OUT}}}(\tau)$ of the NLA output. Such an autocorrelation function can be obtained by means of known closed-form formulas or numerical integration techniques, which require the knowledge of the NLA input statistics, summarized by $R_{u_{\mathrm{IN}}u_{\mathrm{IN}}}(\tau)$, of the input power backoff to the NLA, and of the AM/AM and AM/PM curves that characterize the NLA [10].

After the parallel-to-serial conversion, the signal stream $u_{\mathrm{OUT}}[iP+p] = [\mathbf{u}_{\mathrm{OUT}}[i]]_{p+1}$, $p = 0,\ldots,P-1$, is transmitted through a multipath channel, whose discrete-time equivalent impulse response is

$$h[b] = \sum_{q=1}^{Q} \zeta_q R(bT_{\mathrm{S}} - \tau_q), \tag{4}$$

where Q is the number of paths, ζ_q and τ_q are the complex amplitude and the propagation delay, respectively, of the qth path, $R(\tau)$ is the triangular autocorrelation function of the rectangular pulse-shaping waveform, and $T_{\mathrm{S}} = T/N$ is the sampling period. Throughout the paper, we assume that the channel amplitudes $\{\zeta_q\}$ are zero-mean complex Gaussian random variables, giving rise to Rayleigh fading, and that the maximum delay spread $\tau_{\max} = \max\{\tau_q\}$ is smaller than the cyclic prefix duration $\tau_{\mathrm{CP}} = LT_{\mathrm{S}}$, that is, $h[b]$ may have nonzero entries only for $0 \le b \le L$.

At the receiver side, the samples obtained after matched filtering can be expressed as [12]

$$x[a] = e^{j2\pi f_0 a T_{\mathrm{S}}} \sum_{b=0}^{L} h[b]u_{\mathrm{OUT}}[a-b] + x_{\mathrm{AWGN}}[a], \tag{5}$$

where f_0 is the CFO caused by the frequency synchronization error at the receiver side, $x_{\mathrm{AWGN}}[a]$ represents the AWGN, with $a = iP + p$. Throughout the paper, we assume that the timing information is available at the receiver. In multicarrier systems, such an information could be acquired by exploiting timing synchronization algorithms designed to work in the presence of an unknown CFO [13, 14, 15]. In any case, when timing errors are significant, the BER expressions we will derive can be considered as lower bounds.

The P received samples relative to the gth chip (of the lth symbol) are grouped in the vector $\mathbf{x}[i] = \mathbf{x}[lG+g]$, thus obtaining [12]

$$\mathbf{x}[i] = e^{j2\pi\varepsilon iP/N}\tilde{\mathbf{D}}(\mathbf{H}_0\mathbf{u}_{\mathrm{OUT}}[i] + \mathbf{H}_1\mathbf{u}_{\mathrm{OUT}}[i-1]) + \mathbf{x}_{\mathrm{AWGN}}[i], \tag{6}$$

where $[\mathbf{x}[i]]_{p+1} = x[iP+p]$, $\varepsilon = f_0T$ is the normalized CFO, $\tilde{\mathbf{D}}$ is a $P \times P$ diagonal matrix, defined by $[\tilde{\mathbf{D}}]_{p,p} = \exp(j2\pi\varepsilon(p-1)/N)$, that models the block-independent phase shift introduced by the CFO, and $\mathbf{H}_0$ and $\mathbf{H}_1$ are $P \times P$ Toeplitz matrices defined by [8]

$$\mathbf{H}_0 = \begin{bmatrix} h[0] & 0 & \cdots & \cdots & 0 \\ \vdots & \ddots & \ddots & & \vdots \\ h[L] & & \ddots & \ddots & \vdots \\ \vdots & \ddots & & \ddots & 0 \\ 0 & \cdots & h[L] & \cdots & h[0] \end{bmatrix},$$
$$\mathbf{H}_1 = \begin{bmatrix} 0 & \cdots & h[L] & \cdots & h[1] \\ \vdots & \ddots & & \ddots & \vdots \\ 0 & & \ddots & & h[L] \\ \vdots & \ddots & & \ddots & \vdots \\ 0 & \cdots & 0 & \cdots & 0 \end{bmatrix}. \tag{7}$$

The cyclic prefix elimination, which is common to many multicarrier-based systems, can be represented by the left multiplication of the matrix $\mathbf{R}_{\mathrm{CP}} = [\mathbf{0}_{N\times L} \ \ \mathbf{I}_N]$ with the received vector in (6), which leads to the $N \times 1$ vector [12]

$$\mathbf{y}[i] = \mathbf{R}_{\mathrm{CP}}\mathbf{x}[i] = e^{j2\pi\varepsilon(iP+L)/N}\mathbf{D}\mathbf{R}_{\mathrm{CP}}\mathbf{H}_0\mathbf{u}_{\mathrm{OUT}}[i] + \mathbf{y}_{\mathrm{AWGN}}[i], \tag{8}$$

where $\mathbf{D}$ is an $N \times N$ diagonal matrix defined by $[\mathbf{D}]_{n,n} = \exp(j2\pi\varepsilon(n-1)/N)$, and $\mathbf{y}_{\mathrm{AWGN}}[i] = \mathbf{R}_{\mathrm{CP}}\mathbf{x}_{\mathrm{AWGN}}[i]$ stands for the AWGN term. By using (1) and (2), the vector $\mathbf{y}[i] = \mathbf{y}[lG+g]$ in (8) can also be expressed as

$$\mathbf{y}[lG+g] = e^{j2\pi\varepsilon((lG+g)P+L)/N}\mathbf{D}\mathbf{H}(\alpha\mathbf{F}^H\mathbf{S}[l]\mathbf{c}[g] + \tilde{\mathbf{v}}_{\mathrm{IMD}}[lG+g]) + \mathbf{y}_{\mathrm{AWGN}}[lG+g], \tag{9}$$

where $\mathbf{H} = \mathbf{R}_{\mathrm{CP}}\mathbf{H}_0\mathbf{T}_{\mathrm{CP}}$ is the equivalent channel matrix expressed by $[\mathbf{H}]_{m,n} = h[(m-n)_{\mathrm{mod}\,N}]$, and $\tilde{\mathbf{v}}_{\mathrm{IMD}}[lG+g] = \mathbf{R}_{\mathrm{CP}}\bar{\mathbf{v}}_{\mathrm{IMD}}[lG+g]$. Since $\mathbf{H}$ is circulant, it can be expressed as $\mathbf{H} = \mathbf{F}^H\mathbf{\Lambda}\mathbf{F}$, where $\mathbf{\Lambda} = \mathrm{diag}(\boldsymbol{\lambda})$ is the $N \times N$ diagonal matrix with elements expressed by $\boldsymbol{\lambda} = \sqrt{N}\mathbf{F}\mathbf{h}$, where $\mathbf{h} = [h[0] \ \cdots \ h[N-1]]^T$ and $\boldsymbol{\lambda} = [\lambda_1 \ \cdots \ \lambda_n]^T$ are the channel vectors in the time and frequency domain, respectively. Consequently, the recovery of the transmitted data is accomplished by applying the FFT at the receiver, thus obtaining $\mathbf{z}[lG+g] = \mathbf{F}\mathbf{y}[lG+g]$, which by (9), can be rearranged as

$$\mathbf{z}[lG+g] = e^{j2\pi\varepsilon((lG+g)P+L)/N}\mathbf{\Phi}\mathbf{\Lambda}(\alpha\mathbf{S}[l]\mathbf{c}[g] + \mathbf{v}_{\mathrm{IMD}}[lG+g]) + \mathbf{z}_{\mathrm{AWGN}}[lG+g], \tag{10}$$

where $\mathbf{\Phi} = \mathbf{F}\mathbf{D}\mathbf{F}^H$ is the $N \times N$ circulant matrix that models the ICI due to the CFO, $\mathbf{v}_{\mathrm{IMD}}[lG+g] = \mathbf{F}\tilde{\mathbf{v}}_{\mathrm{IMD}}[lG+g]$ is the IMD after the FFT operation, and $\mathbf{z}_{\mathrm{AWGN}}[lG+g] = \mathbf{F}\mathbf{y}_{\mathrm{AWGN}}[lG+g]$ represents the AWGN after the FFT operation.

Due to the spreading in the time domain, in order to decode the N data symbols $\mathbf{s}_k[l] = [s_{1,k}[l] \ \cdots \ s_{N,k}[l]]^T$ relative

to the lth interval, the receiver of the kth user has to collect G consecutive chip vectors $\{\mathbf{z}[lG+g]\}_{g=0,\ldots,G-1}$ in (10). By defining the $N\times G$ matrices

$$\begin{aligned}\mathbf{Z}[l] &= \Big[\mathbf{z}[lG] \;\cdots\; \mathbf{z}[lG+G-1]\Big],\\ \mathbf{V}_{\mathrm{IMD}}[l] &= \Big[\mathbf{v}_{\mathrm{IMD}}[lG] \;\cdots\; \mathbf{v}_{\mathrm{IMD}}[lG+G-1]\Big],\\ \mathbf{Z}_{\mathrm{AWGN}}[l] &= \Big[\mathbf{z}_{\mathrm{AWGN}}[lG] \;\cdots\; \mathbf{z}_{\mathrm{AWGN}}[lG+G-1]\Big],\end{aligned} \tag{11}$$

from (10), we obtain

$$\mathbf{Z}[l] = e^{j2\pi\varepsilon L/N}\boldsymbol{\Phi}\boldsymbol{\Lambda}(\alpha\mathbf{S}[l]\mathbf{C}+\mathbf{V}_{\mathrm{IMD}}[l])\mathbf{E}[l]+\mathbf{Z}_{\mathrm{AWGN}}[l], \tag{12}$$

where $\mathbf{C} = [\mathbf{c}[0] \;\cdots\; \mathbf{c}[G-1]] = [\mathbf{c}_1 \;\mathbf{c}_2 \;\cdots\; \mathbf{c}_K]^T$ is the $K\times G$ matrix whose rows contain the spreading codes of the K users, and $\mathbf{E}[l]$ is a $G\times G$ diagonal matrix defined as $[\mathbf{E}[l]]_{g+1,g+1} = e^{j2\pi\varepsilon(lG+g)P/N}$, $g = 0,\ldots,G-1$.

The matrix model expressed by (12) allows a nice representation of the MC-DS-CDMA received signal. Indeed, the number of rows of $\mathbf{Z}[l]$ in (12) is equal to the number of subcarriers, while the number of columns of $\mathbf{Z}[l]$ is equal to the processing gain. Consequently, we are able to represent linear frequency-domain operations (such as the equalization) by matrix multiplications on the left-hand side of $\mathbf{Z}[l]$, and linear time-domain operations (such as the despreading) by matrix multiplications on the right-hand side of $\mathbf{Z}[l]$.

Expression (12) shows the effects of both nonlinear distortions and frequency synchronization errors on the spread data matrix $\mathbf{S}[l]\mathbf{C}$. Specifically, the NLA introduces the constant complex gain α and the additive term $\mathbf{V}_{\mathrm{IMD}}[l]$, which represents the IMD. Moreover, the NLA-distorted signal, after passing through the multipath channel summarized by the diagonal matrix $\boldsymbol{\Lambda}$, is affected by the CFO-induced ICI, because the matrix $\boldsymbol{\Phi}$ is not diagonal. In addition, the CFO produces two phase-shift effects. The first one is a time-invariant phase shift $\varphi = e^{j2\pi\varepsilon L/N}e^{j\pi\varepsilon(N-1)/N}$ (the factor $e^{j\pi\varepsilon(N-1)/N}$ is contained in the main diagonal of $\boldsymbol{\Phi}$), which adds to the phase shift caused by the NLA. The second effect is a time-varying phase shift, which is represented by the diagonal matrix $\mathbf{E}[l]$. In this paper, we assume that the receiver is able to perfectly compensate for the time-invariant phase-shift term φ, which could also be seen as part of the channel-induced distortion. As far as the compensation for the time-variant phase shift is concerned, we consider two alternative hypotheses.

Hypothesis H1

The receiver obtains an accurate phase-shift estimate in each chip interval, as assumed in [6]. As a consequence, by the knowledge of $\mathbf{E}[l]$ at the receiver side, the estimated phase-shift matrix can be expressed by $\hat{\mathbf{E}}[l] = \hat{\mathbf{E}}[l]_{\mathrm{H1}} = \mathbf{E}[l]$.

Hypothesis H2

The receiver does not track the time-variant phase shift at the chip level, estimating only the average phase shift within a symbol interval. Hence, by the knowledge of the mean of the elements in $\mathbf{E}[l]$, the estimated phase-shift matrix $\hat{\mathbf{E}}[l] = \hat{\mathbf{E}}[l]_{\mathrm{H2}}$ is diagonal, with elements

$$\begin{aligned}\left[\hat{\mathbf{E}}[l]_{\mathrm{H2}}\right]_{g+1,g+1} &= \exp\left(j\frac{1}{G}\sum_{g=0}^{G-1}\frac{2\pi\varepsilon(lG+g)P}{N}\right)\\ &= \exp\left(j\frac{2\pi\varepsilon P}{N}\left(lG+\frac{G-1}{2}\right)\right).\end{aligned} \tag{13}$$

It can be noted that the perfect knowledge of the phase shifts is not completely realistic. However, we consider this hypothesis because it produces a lower bound that is independent of the phase-shift estimation technique.

In this paper, we assume that the receiver performs a single-tap frequency-domain equalization and code despreading. In the absence of NLA- and CFO-induced impairments, the equalizer-despreader detector is able to eliminate both ISI and MAI when orthogonal spreading codes are employed. From the computational complexity point of view, the equalizer-despreader detector is less demanding than multiuser detectors [5], and hence it seems to be more suitable in the downlink situation.

The receiver can perform the despreading operation after the phase-shift compensation and the channel equalization. Thus, by assuming perfect channel state information (CSI) at the receiver side, the equalized data matrix can be constructed as $\mathbf{Z}_{\mathrm{EQ}}[l] = \varphi^*\alpha^{-1}\boldsymbol{\Lambda}^{-1}\mathbf{Z}[l]\hat{\mathbf{E}}[l]^{-1}$. From (12), $\mathbf{Z}_{\mathrm{EQ}}[l]$ becomes equal to

$$\mathbf{Z}_{\mathrm{EQ}}[l] = \boldsymbol{\Lambda}^{-1}\mathbf{M}\boldsymbol{\Lambda}\mathbf{S}[l]\mathbf{C}\boldsymbol{\Theta}+\mathbf{Z}_{\mathrm{EQ,IMD}}[l]+\mathbf{Z}_{\mathrm{EQ,AWGN}}[l], \tag{14}$$

where $\mathbf{M} = e^{-j\pi\varepsilon(N-1)/N}\boldsymbol{\Phi}$ represents the phase-compensated ICI matrix, $\mathbf{Z}_{\mathrm{EQ,IMD}}[l] = \alpha^{-1}\boldsymbol{\Lambda}^{-1}\mathbf{M}\boldsymbol{\Lambda}\mathbf{V}_{\mathrm{IMD}}[l]\boldsymbol{\Theta}$ represent the IMD after the channel equalization, $\mathbf{Z}_{\mathrm{EQ,AWGN}}[l] = \varphi^*\alpha^{-1}\boldsymbol{\Lambda}^{-1}\mathbf{Z}_{\mathrm{AWGN}}[l]\hat{\mathbf{E}}[l]^{-1}$, and $\boldsymbol{\Theta} = \mathbf{E}[l]\hat{\mathbf{E}}[l]^{-1}$ is a diagonal matrix equal to $\boldsymbol{\Theta}_{\mathrm{H1}} = \mathbf{I}_G$ under Hypothesis H1, and defined as $[\boldsymbol{\Theta}_{\mathrm{H2}}]_{g+1,g+1} = \exp(j(2\pi\varepsilon P/N)(g-(G-1)/2))$ under Hypothesis H2. The despreading operation leads to an N-dimensional vector that contains the N decision variables of the kth user, as expressed by

$$\begin{aligned}\mathbf{z}_{\mathrm{DESPR},k}[l] &= \mathbf{Z}_{\mathrm{EQ}}[l]\mathbf{c}_k^*\\ &= \boldsymbol{\Lambda}^{-1}\mathbf{M}\boldsymbol{\Lambda}\mathbf{S}[l]\mathbf{C}\boldsymbol{\Theta}\mathbf{c}_k^*+\mathbf{z}_{\mathrm{DESPR},k,\mathrm{IMD}}[l]\\ &\quad+\mathbf{z}_{\mathrm{DESPR},k,\mathrm{AWGN}}[l],\end{aligned} \tag{15}$$

where $\mathbf{z}_{\mathrm{DESPR},k,\mathrm{IMD}}[l] = \mathbf{Z}_{\mathrm{EQ,IMD}}[l]\mathbf{c}_k^*$, and $\mathbf{z}_{\mathrm{DESPR},k,\mathrm{AWGN}}[l] = \mathbf{Z}_{\mathrm{EQ,AWGN}}[l]\mathbf{c}_k^*$. The decision over $\mathbf{z}_{DESPR,k}[l]$ is successively done according to the proper constellation size M.

It should be pointed out that the K-dimensional vector $\mathbf{C}\boldsymbol{\Theta}\mathbf{c}_k^*$ represents the effect of the CFO-induced time-varying phase shift on the spreading-despreading operation. If the time-varying phase shift can be perfectly compensated for, that is, under Hypothesis H1, this vector becomes equal to $\mathbf{C}\mathbf{c}_k^*$. Therefore, if the users employ orthogonal spreading codes, the multiuser interference has been perfectly eliminated, because the product $\mathbf{S}[l]\mathbf{C}\boldsymbol{\Theta}_{\mathrm{H1}}\mathbf{c}_k^*$ in (15) is equal to $\mathbf{s}_k[l]$. On the contrary, under Hypothesis H2, the multiuser interference cannot be completely eliminated.

Indeed, when $k' \neq k$, we have

$$\begin{aligned}\rho_{k,k',\mathrm{H2}} &= \left[\mathbf{C}\boldsymbol{\Theta}_{\mathrm{H2}}\mathbf{c}_k^*\right]_{k'} \\ &= \mathbf{c}_{k'}^T\boldsymbol{\Theta}_{\mathrm{H2}}\mathbf{c}_k^* \\ &= \sum_{g=0}^{G-1} e^{j(2\pi\varepsilon P/N)(g-(G-1)/2)} c_{k',g}c_{k,g}^*,\end{aligned} \tag{16}$$

which is, in general, different from zero even for orthogonal sequences (characterized by $\mathbf{c}_{k'}^T\mathbf{c}_k^* = \sum_{g=0}^{G-1} c_{k',g}c_{k,g}^* = 0$). An interesting matter could be the search for spreading sequences that minimize (16), following the lines suggested by [16]. However, this topic is beyond the scope of this paper.

Furthermore, since $\rho_{k,k,\mathrm{H2}} = \mathbf{c}_k^T\boldsymbol{\Theta}_{\mathrm{H2}}\mathbf{c}_k^* < 1$, the time-variant phase shift also introduces an attenuation factor of the useful signal, given by

$$\rho_{k,k,\mathrm{H2}} = \frac{1}{G}\sum_{g=0}^{G-1} e^{j(2\pi\varepsilon P/N)(g-(G-1)/2)} = \frac{\sin(\pi\varepsilon PG/N)}{G\sin(\pi\varepsilon P/N)}. \tag{17}$$

For a given maximum tolerable frequency offset ε, the attenuation factor in (17) limits the maximum value G of the processing gain. Indeed, $\rho_{k,k,\mathrm{H2}}$ is close to 1 only if $\varepsilon \ll N/(N+L)G \approx 1/G$. On the contrary, under Hypothesis H1, $\rho_{k,k,\mathrm{H1}} = \mathbf{c}_k^T\boldsymbol{\Theta}_{\mathrm{H1}}\mathbf{c}_k^* = 1$, and hence no attenuation is introduced by the spreading-despreading operation. It should be observed that $\rho_{k,k}$ is independent of the user index k in both hypotheses, and hence, in the following, it will be denoted by ρ.

3. BER OF MC-DS-CDMA SYSTEMS IN FLAT-FADING CHANNELS

In this section, we evaluate the effect of the previously described impairments when the channel exhibits flat-fading behavior. The results herein obtained will be useful for the performance evaluation in frequency-selective fading channels, developed in the next section. In the flat-fading case, all the subcarriers experience the same channel gain. Consequently, since $\boldsymbol{\Lambda} = \lambda\mathbf{I}_N$, (15) can be simplified to

$$\begin{aligned}\mathbf{z}_{\mathrm{DESPR},k}[l] = {}& \mathbf{M}\mathbf{S}[l]\mathbf{C}\boldsymbol{\Theta}\mathbf{c}_k^* + \alpha^{-1}\mathbf{M}\mathbf{V}_{\mathrm{IMD}}[l]\boldsymbol{\Theta}\mathbf{c}_k^* \\ &+ \varphi^*\alpha^{-1}\lambda^{-1}\mathbf{Z}_{\mathrm{AWGN}}[l]\hat{\mathbf{E}}[l]^{-1}\mathbf{c}_k^*.\end{aligned} \tag{18}$$

For convenience, we consider the scaled version of (18) obtained by multiplying $\mathbf{z}_{\mathrm{DESPR},k}[l]$ with $\lambda|\alpha|$. Therefore, we obtain $\mathbf{z}_{\mathrm{SC},k}[l] = \lambda|\alpha|\mathbf{z}_{\mathrm{DESPR},k}[l]$, and, by focusing on the nth subcarrier, it yields

$$\begin{aligned}z_{\mathrm{SC},n,k}[l] &= \left[\mathbf{z}_{\mathrm{SC},k}[l]\right]_n \\ &= \lambda|\alpha|\mathbf{m}_n^T\mathbf{S}[l]\mathbf{C}\boldsymbol{\Theta}\mathbf{c}_k^* \\ &\quad + \lambda e^{-j\arg(\alpha)}\mathbf{m}_n^T\mathbf{V}_{\mathrm{IMD}}[l]\boldsymbol{\Theta}\mathbf{c}_k^* \\ &\quad + \varphi^* e^{-j\arg(\alpha)}\mathbf{z}_{n,\mathrm{AWGN}}[l]^T\hat{\mathbf{E}}[l]^{-1}\mathbf{c}_k^*,\end{aligned} \tag{19}$$

where $\mathbf{z}_{n,\mathrm{AWGN}}[l]^T$ is the nth row of $\mathbf{Z}_{\mathrm{AWGN}}[l]$, and $\mathbf{m}_n = [m_{n,1} \ \cdots \ m_{n,N}]^T$ collects the elements on the nth row of $\mathbf{M}$. It can be verified that [17]

$$\begin{aligned}m_{n,n'} &= [\mathbf{M}]_{n,n'} \\ &= \frac{\sin\left(\pi\left((n'-n)_{\mathrm{mod}\,N} + \varepsilon\right)\right)}{N\sin\left((\pi/N)\left((n'-n)_{\mathrm{mod}\,N} + \varepsilon\right)\right)} \\ &\quad \times e^{j\pi((N-1)/N)(n'-n)_{\mathrm{mod}\,N}},\end{aligned} \tag{20}$$

where $m_{n,n'}$ represents the ICI coefficient relative to the n'th subcarrier when $n' \neq n$, and an additional attenuation factor, denoted by $m = m_{n,n}$, when $n' = n$. Since $\mathbf{S}[l]\mathbf{C}\boldsymbol{\Theta}\mathbf{c}_k^* = \rho\mathbf{s}_k[l] + \sum_{\substack{k'=1\\k'\neq k}}^{K}\rho_{k,k'}\mathbf{s}_{k'}[l]$, by dropping the symbol index l for the sake of simplicity, (19) can be rewritten as

$$\begin{aligned}z_{\mathrm{SC},n,k} = {}& \lambda\left(|\alpha|\rho m s_{n,k} + z_{\mathrm{ICI},n,k} + z_{\mathrm{MAI},n,k} + z_{\mathrm{MAICI},n,k} + z_{\mathrm{IMD},n,k}\right) \\ &+ z_{\mathrm{AWGN},n,k},\end{aligned} \tag{21}$$

where

$$z_{\mathrm{ICI},n,k} = |\alpha|\rho\sum_{\substack{n'=1\\n'\neq n}}^{N} m_{n,n'}s_{n',k} \tag{22}$$

represents the ICI coming from the symbols of the kth user,

$$z_{\mathrm{MAI},n,k} = |\alpha|m\sum_{\substack{k'=1\\k'\neq k}}^{K}\rho_{k,k'}s_{n,k'} \tag{23}$$

represents the MAI coming from the symbols of the other users on the nth subcarrier,

$$z_{\mathrm{MAICI},n,k} = |\alpha|\sum_{\substack{k'=1\\k'\neq k}}^{K}\rho_{k,k'}\sum_{\substack{n'=1\\n'\neq n}}^{N} m_{n,n'}s_{n',k'} \tag{24}$$

represents the multiple-access ICI (MAICI) coming from the symbols of the other users on the other subcarriers,

$$z_{\mathrm{IMD},n,k} = e^{-j\arg(\alpha)}\mathbf{m}_n^T\mathbf{V}_{\mathrm{IMD}}\boldsymbol{\Theta}\mathbf{c}_k^* \tag{25}$$

represents the IMD, and

$$z_{\mathrm{AWGN},n,k} = \varphi^* e^{-j\arg(\alpha)}\mathbf{z}_{n,\mathrm{AWGN}}^T\hat{\mathbf{E}}^{-1}\mathbf{c}_k^* \tag{26}$$

represents the AWGN.

In order to find the BER of the kth user on the nth subcarrier, we will firstly evaluate the conditional bit-error probability $P_{\mathrm{BE},n,k}(\lambda)$ for a given channel gain λ, and we will successively average the obtained $P_{\mathrm{BE},n,k}(\lambda)$ over the probability density function (pdf) $f_\lambda(\lambda)$ of the channel gain.

Therefore, we will determine the BER by making use of the expressions

$$(\mathrm{BER})_{n,k} = \int_{\lambda} P_{\mathrm{BE},n,k}(\lambda) f_{\lambda}(\lambda) d\lambda, \tag{27}$$

$$P_{\mathrm{BE},n,k}(\lambda) = \int_{\mathbf{S}} P_{\mathrm{BE},n,k}(\mathbf{S},\lambda) f_{\mathbf{S}}(\mathbf{S}) d\mathbf{S}, \tag{28}$$

where $P_{\mathrm{BE},n,k}(\mathbf{S},\lambda)$ is the bit-error probability conditioned on both the channel gain λ and the data symbols in $\mathbf{S}[l]$, and $f_{\mathbf{S}}(\mathbf{S})$ is the multidimensional pdf of the data symbols in $\mathbf{S}[l]$.

3.1. Conditional bit-error probability evaluation

From (21), we observe that we have five noise terms, each one with different statistical characterization. Hence, the computation of the conditional probability $P_{\mathrm{BE}}(\lambda)$ seems to be quite complicated. As a consequence, a reasonable way to proceed relies on finding simple (yet accurate) approximations that allow a mathematical treatment. Along this way, we observe that the ICI term $z_{\mathrm{ICI},n,k}$ in (22) is obtained by the linear combination of $N-1$ symbols, each one weighted by a different coefficient $m_{n,n'}$. If the frequency offset ε is not too high (e.g., $\varepsilon < 0.1$), the coefficients $\{m_{n,n'}\}_{n\neq n'}$ have comparable amplitudes. Therefore, under the hypothesis of high number N of subcarriers, the ICI term in (22) can be well approximated by a zero-mean Gaussian random variable with power

$$\begin{aligned}\sigma^2_{\mathrm{ICI},n,k} &= |\alpha\rho|^2 \sum_{\substack{n'=1\\ n'\neq n}}^{N} |m_{n,n'}|^2 \sigma_S^2 \\ &= |\alpha\rho|^2 \left(1 - \frac{\sin^2(\pi\varepsilon)}{N^2 \sin^2(\pi\varepsilon/N)}\right)\sigma_S^2.\end{aligned} \tag{29}$$

We want also to underline that both the hypotheses of high N and low CFO seem to be realistic. Indeed, multicarrier systems usually employ many active subcarriers, from $N = 52$ in WLAN environments to $N \approx 6000$ in broadcasting applications [18]. Moreover, in the presence of high CFO, the BER will be very high (e.g., BER > 0.1), and therefore in this case the BER analysis seems to be of limited practical interest.

It should be pointed out that the ICI power in (29) does not depend on the user index k as long as σ_S^2 remains the same for all the users, as assumed in this paper. However, the results could be extended to take into account different user powers. Moreover, our BER analysis can be easily extended in order to take into account the presence of N_{VS} switched-off subcarriers that are used as guard frequency bands, because a switched-off subcarrier does not contribute to the ICI and to the MAICI. Therefore, the BER analysis remains still valid, provided that the various summations over the subcarrier index n' (e.g., (22), (24), etc.) consider only the active subcarriers.

As far as the MAI term is concerned, we similarly observe that $z_{\mathrm{MAI},n,k}$ in (23) is obtained as the sum of the $K-1$ elements $\{s_{k',n}\}$, weighted by almost equal elements $\{\rho_{k,k'}\}$. Therefore, when the number K of users is sufficiently high, we can exploit the Gaussian approximation as we did for the ICI term. The MAI power can be expressed as

$$\sigma^2_{\mathrm{MAI},n,k} = |\alpha m|^2 \sum_{\substack{k'=1\\ k'\neq k}}^{K} |\rho_{k,k'}|^2 \sigma_S^2. \tag{30}$$

Since high bit rates are expected in the downlink of fourth generation (4G) systems, also the hypothesis of high K seems to be realistic, because many spreading codes can be assigned to the same user in order to provide higher bit rates (multicode transmission). Therefore, K can be interpreted as the number of spreading codes assigned to $\tilde{K}$ active users, with $\tilde{K} < K$. Moreover we remark that, under Hypothesis H1, the MAI term can be set to zero by employing orthogonal codes, and hence no accurate MAI characterization is necessary in this case.

Because of the previous assumptions about the number K of equivalent users and the number N of subcarriers, the MAICI term can be approximated by a zero-mean Gaussian variable as well, with power equal to

$$\begin{aligned}\sigma^2_{\mathrm{MAICI},n,k} &= |\alpha|^2 \sum_{\substack{k'=1\\ k'\neq k}}^{K} |\rho_{k,k'}|^2 \sum_{\substack{n'=1\\ n'\neq n}}^{N} |m_{n,n'}|^2 \sigma_S^2 \\ &= |\alpha|^2 \sum_{\substack{k'=1\\ k'\neq k}}^{K} |\rho_{k,k'}|^2 \left(1 - \frac{\sin^2(\pi\varepsilon)}{N^2 \sin^2(\pi\varepsilon/N)}\right)\sigma_S^2.\end{aligned} \tag{31}$$

We remark that, under Hypothesis H1, also the MAICI term vanishes when the codes are orthogonal.

We also observe that the IMD term $z_{\mathrm{IMD},n,k}$ in (25) can equivalently be expressed as $z_{\mathrm{IMD},n,k} = \sum_{g=0}^{G-1} e^{-j\arg(\alpha)} \theta_{g+1} c^*_{k,g} \mathbf{m}_n^T \mathbf{v}_{\mathrm{IMD},g}$, where $\theta_{g+1} = [\boldsymbol{\Theta}]_{g+1,g+1}$, and $\mathbf{v}_{\mathrm{IMD},g}$ is the gth column of $\mathbf{V}_{\mathrm{IMD}}$. Since $\mathbf{V}_{\mathrm{IMD}}$ is evaluated at the output of the receiver FFT, the assumption of high N allows to approximate the pdf of $\mathbf{v}_{\mathrm{IMD},g}$ as a multidimensional Gaussian pdf. Moreover, $\mathbf{V}_{\mathrm{IMD}}$ is transformed in $z_{\mathrm{IMD},n,k}$ by linear operations, and hence $z_{\mathrm{IMD},n,k}$ also can be modeled as a zero-mean Gaussian random variable, with power expressed by

$$\sigma^2_{\mathrm{IMD},n,k} = \sum_{g=0}^{G-1} \sum_{g'=0}^{G-1} \theta_{g+1} \theta^*_{g'+1} c^*_{k,g} c_{k,g'} \mathbf{m}_n^T \mathbf{R}_{\mathbf{v}}(g,g') \mathbf{m}_n^*, \tag{32}$$

where

$$\mathbf{R}_{\mathbf{v}}(g,g') = E\{\mathbf{v}_{\mathrm{IMD},g} \mathbf{v}^H_{\mathrm{IMD},g'}\} = \mathbf{F}\mathbf{R}_{\mathrm{CP}} \mathbf{R}_{\tilde{\mathbf{v}}}(g,g') \mathbf{R}^T_{\mathrm{CP}} \mathbf{F}^H, \tag{33}$$

which depends on the indexes g and g', can be calculated by exploiting the knowledge of the IMD autocorrelation function, summarized by $\mathbf{R}_{\tilde{\mathbf{v}}}(g,g')$ in (3).

Since the interference terms in (21) are modeled as zero-mean Gaussian random variables, also the aggregate noise can be considered as Gaussian. Indeed, the data of different users or different subcarriers are uncorrelated with one another, as well as the ICI, the MAI, and the MAICI terms are uncorrelated with one another and with the useful signal. Moreover, thanks to the Bussgang theorem, the IMD term also is uncorrelated with the other terms. Consequently, the power of the aggregate noise is equal to the sum of the powers of the individual noise terms. Hence, the conditional bit-error probability $P_{\mathrm{BE},n,k}(\lambda)$, for square M-QAM with Gray coding, can be expressed by [19]

$$P_{\mathrm{BE},n,k}(\lambda) = \frac{1}{\log_2\sqrt{M}} \sum_{q=1}^{\log_2\sqrt{M}} P_{n,k}(q,\lambda),$$

$$P_{n,k}(q,\lambda) = \frac{1}{\sqrt{M}} \times \sum_{i=0}^{(1-2^{-q})\sqrt{M}-1} \left\{ (-1)^{\lfloor 2^{q-1} i/\sqrt{M} \rfloor} \left(2^q - 2\left\lfloor \frac{2^{q-1} i}{\sqrt{M}} - \frac{1}{2} \right\rfloor \right) \times Q\left((2i+1)\sqrt{\frac{3}{M-1}\gamma_{n,k}(\lambda)} \right) \right\}, \tag{34}$$

with the signal-to-interference-plus-noise ratio (SINR) $\gamma_{n,k}(\lambda)$ expressed by

$$\gamma_{n,k}(\lambda) = \frac{|\lambda|^2 |\alpha\rho m|^2 \sigma_{\mathrm{S}}^2}{|\lambda|^2 \left(\sigma_{\mathrm{ICI},n,k}^2 + \sigma_{\mathrm{MAI},n,k}^2 + \sigma_{\mathrm{MAICI},n,k}^2 + \sigma_{\mathrm{IMD},n,k}^2\right) + \sigma_{\mathrm{AWGN}}^2}. \tag{35}$$

3.2. Average over the channel statistics

For convenience, we rewrite (34) as

$$P_{\mathrm{BE},n,k}(\lambda) = \sum_{i=0}^{\sqrt{M}-2} a_i Q\left(\sqrt{b_i \gamma_{n,k}(\lambda)} \right), \tag{36}$$

where the coefficients $\{a_i\}$ and $\{b_i\}$, calculated from (34), depend on the modulation size M. Therefore, the resultant BER, which is obtained by inserting in (27) the expressions (35), (36), and the specific pdf $f_\lambda(\lambda)$ of the channel, can be expressed as the sum of $\sqrt{M}-1$ integrals. Each integral can then be evaluated by numerical techniques.

We want to highlight that such an approach can be used regardless of the statistical characterization of the channel. However, when the channel is characterized by Rayleigh fading (i.e., $f_{|\lambda|}(\lambda) = (2|\lambda|/\sigma_\lambda^2) e^{-|\lambda|^2/\sigma_\lambda^2}$, $\lambda > 0$), as assumed in this paper, we can circumvent the numerical integration by evaluating a suitable series expansion. As an example, for 4-QAM, (36) becomes $P_{\mathrm{BE},n,k}(\lambda) = Q(\sqrt{\gamma_{n,k}(\lambda)})$, and consequently (27) becomes [20, 21]

$$\begin{aligned}(\mathrm{BER})_{n,k} &= \int_0^{+\infty} Q\left(\sqrt{\gamma(\lambda)}\right) \frac{2|\lambda|}{\sigma_\lambda^2} e^{-|\lambda|^2/\sigma_\lambda^2} d|\lambda| \\ &= \frac{1}{2} - \frac{\sqrt{2\mu_{n,k}^2}}{4} e^{-\mu_{n,k}^2/2\nu_{n,k}^2} \sum_{i=0}^{+\infty} \frac{1}{i!} \left(\frac{\mu_{n,k}^2}{2\nu_{n,k}^2} \right)^i \\ &\quad \times {}_2F_0\left(i+\frac{3}{2}, \frac{1}{2}; ; -\nu_{n,k}^2 \right),\end{aligned} \tag{37}$$

where ${}_pF_q(\cdot;\cdot;\cdot)$ denotes the generalized hypergeometric function [22], and $\mu_{n,k}^2$ and $\nu_{n,k}^2$ are expressed by

$$\begin{aligned}\mu_{n,k}^2 = \mu^2 &= \frac{|\alpha\rho m|^2 \sigma_{\mathrm{S}}^2 \sigma_\lambda^2}{\sigma_{\mathrm{AWGN}}^2}, \\ \nu_{n,k}^2 &= \frac{\left(\sigma_{\mathrm{ICI},n,k}^2 + \sigma_{\mathrm{MAI},n,k}^2 + \sigma_{\mathrm{MAICI},n,k}^2 + \sigma_{\mathrm{IMD},n,k}^2\right)\sigma_\lambda^2}{\sigma_{\mathrm{AWGN}}^2}.\end{aligned} \tag{38}$$

As a consequence of (36) and (37), the general M-QAM case leads to a BER that is expressed as the sum of $\sqrt{M}-1$ series expansions. Note that each series expansion in the form of (37) can be conveniently truncated without affecting significantly the BER value (see [21] for a simple and accurate truncation criterion).

4. BER OF MC-DS-CDMA SYSTEMS IN FREQUENCY-SELECTIVE CHANNELS

For frequency-selective fading channels, we will follow a two-step approach similar to that adopted for frequency-flat channels. By denoting by $\lambda_n = [\mathbf{\Lambda}]_{n,n}$ the channel gain of the nth subcarrier, the frequency-selective counterparts of (27) and (28) can be expressed by

$$(\mathrm{BER})_{n,k} = \int_{\lambda_n} P_{\mathrm{BE},n,k}(\lambda_n) f_{\lambda_n}(\lambda_n) d\lambda_n, \tag{39}$$

$$P_{\mathrm{BE},n,k}(\lambda_n) = \int_{\mathbf{S},\bar{\boldsymbol{\lambda}}_n} P_{\mathrm{BE},n,k}(\mathbf{S},\boldsymbol{\lambda}) f_{\bar{\boldsymbol{\lambda}}_n|\lambda_n}(\bar{\boldsymbol{\lambda}}_n|\lambda_n) f_{\mathbf{S}}(\mathbf{S}) d\mathbf{S}\, d\bar{\boldsymbol{\lambda}}_n, \tag{40}$$

where $f_{\lambda_n}(\lambda_n)$ is the pdf of λ_n, $f_{\bar{\boldsymbol{\lambda}}_n|\lambda_n}(\bar{\boldsymbol{\lambda}}_n|\lambda_n)$ is the conditional pdf of the channel vector

$$\bar{\boldsymbol{\lambda}}_n = \begin{bmatrix} \lambda_1 & \cdots & \lambda_{n-1} & \lambda_{n+1} & \cdots & \lambda_N \end{bmatrix}^T \tag{41}$$

of the other subcarriers given the subcarrier of interest λ_n, and $P_{\mathrm{BE},n,k}(\mathbf{S},\boldsymbol{\lambda})$ is the bit-error probability conditioned on both the channel gains in $\boldsymbol{\lambda}$ and the data symbols in $\mathbf{S}[l]$. By multiplying (15) with $\lambda_n|\alpha|$, the scaled decision variable $z_{\mathrm{SC},n,k}[l]$ can be expressed by

$$\begin{aligned}z_{\mathrm{SC},n,k}[l] = {} & |\alpha| \mathbf{m}_n^T \mathbf{\Lambda} \mathbf{S}[l] \mathbf{C} \mathbf{\Theta} \mathbf{c}_k^* + e^{-j\arg(\alpha)} \mathbf{m}_n^T \mathbf{\Lambda} \mathbf{V}_{\mathrm{IMD}}[l] \mathbf{\Theta} \mathbf{c}_k^* \\ & + \varphi^* e^{-j\arg(\alpha)} \mathbf{z}_{n,\mathrm{AWGN}}[l]^T \hat{\mathbf{E}}[l]^{-1} \mathbf{c}_k^*.\end{aligned} \tag{42}$$

By exploiting $\mathbf{S}[l]\mathbf{C}\boldsymbol{\Theta}\mathbf{c}_k^* = \rho\mathbf{s}_k[l] + \sum_{\substack{k'=1\\k'\neq k}}^{K}\rho_{k,k'}\mathbf{s}_{k'}[l]$, and dropping the index l, (42) becomes

$$\begin{aligned} z_{\mathrm{SC},n,k} &= |\alpha|\rho m\lambda_n s_{n,k} + |\alpha|\rho\sum_{\substack{n'=1\\n'\neq n}}^{N} m_{n,n'}\lambda_{n'}s_{n',k} \\ &\quad + |\alpha|m\lambda_n\sum_{\substack{k'=1\\k'\neq k}}^{K}\rho_{k,k'}s_{n,k'} \\ &\quad + |\alpha|\sum_{\substack{n'=1\\n'\neq n}}^{N} m_{n,n'}\lambda_{n'}\sum_{\substack{k'=1\\k'\neq k}}^{K}\rho_{k,k'}s_{n',k'} \\ &\quad + \sum_{g=0}^{G-1} e^{-j\arg(\alpha)}\theta_{g+1}c_{k,g}^*\sum_{n'=1}^{N} m_{n,n'}\lambda_{n'}\nu_{\mathrm{IMD},n',g} \\ &\quad + z_{\mathrm{AWGN},n,k}, \end{aligned} \tag{43}$$

where $\nu_{\mathrm{IMD},n,g}$ is the (n,g)th element of $\mathbf{V}_{\mathrm{IMD}}$, and $z_{\mathrm{AWGN},n,k} = \varphi^* e^{-j\arg(\alpha)}\mathbf{z}_{n,\mathrm{AWGN}}^T\hat{\mathbf{E}}^{-1}\mathbf{c}_k^*$. Equation (43) clearly illustrates the presence of the interference terms (ICI, MAI, MAICI, and IMD). By constructing the conditional random variable $t_{\mathrm{SC},n,k} = z_{\mathrm{SC},n,k}|\lambda_n$, from (43), we obtain

$$\begin{aligned} t_{\mathrm{SC},n,k} &= \lambda_n|\alpha|\rho m s_{n,k} + |\alpha|\rho\sum_{\substack{n'=1\\n'\neq n}}^{N} m_{n,n'}\hat{\lambda}_{n',n}s_{n',k} \\ &\quad + \lambda_n|\alpha|m\sum_{\substack{k'=1\\k'\neq k}}^{K}\rho_{k,k'}s_{n,k'} \\ &\quad + |\alpha|\sum_{\substack{n'=1\\n'\neq n}}^{N} m_{n,n'}\hat{\lambda}_{n',n}\sum_{\substack{k'=1\\k'\neq k}}^{K}\rho_{k,k'}s_{n',k'} \\ &\quad + \lambda_n e^{-j\arg(\alpha)}m\sum_{g=0}^{G-1}\theta_{g+1}c_{k,g}^*\nu_{\mathrm{IMD},n,g} \\ &\quad + e^{-j\arg(\alpha)}\sum_{g=0}^{G-1}\theta_{g+1}c_{k,g}^*\sum_{\substack{n'=1\\n'\neq n}}^{N} m_{n,n'}\hat{\lambda}_{n',n}\nu_{\mathrm{IMD},n',g} \\ &\quad + z_{\mathrm{AWGN},n,k}, \end{aligned} \tag{44}$$

where $\hat{\lambda}_{n',n} = \lambda_{n'}|\lambda_n$ is the random variable that indicates the channel gain value on the n'th subcarrier conditioned on the channel gain on the nth subcarrier. Note that in (44) the IMD relative to the subcarrier of interest and the IMD coming from the other subcarriers are considered separately. As shown in [23, page 532], the $(N-1)\times 1$ vector $\hat{\boldsymbol{\lambda}}_n = [\hat{\lambda}_{1,n}\ \cdots\ \hat{\lambda}_{n-1,n}\ \hat{\lambda}_{n+1,n}\ \cdots\ \hat{\lambda}_{N,n}]^T$ is still a Gaussian random vector, with mean value $\boldsymbol{\eta}_{\hat{\boldsymbol{\lambda}}_n} = E\{\hat{\boldsymbol{\lambda}}_n\}$ and covariance $\mathbf{R}_{\hat{\boldsymbol{\lambda}}_n} = E\{\hat{\boldsymbol{\lambda}}_n\hat{\boldsymbol{\lambda}}_n^H\}$ expressed by

$$\begin{aligned} \boldsymbol{\eta}_{\hat{\boldsymbol{\lambda}}_n} &= \lambda_n r_{\lambda_n\lambda_n}^{-1}\mathbf{r}_{\bar{\boldsymbol{\lambda}}_n\lambda_n}, \\ \mathbf{R}_{\hat{\boldsymbol{\lambda}}_n} &= \mathbf{R}_{\bar{\boldsymbol{\lambda}}_n} - r_{\lambda_n\lambda_n}^{-1}\mathbf{r}_{\bar{\boldsymbol{\lambda}}_n\lambda_n}\mathbf{r}_{\bar{\boldsymbol{\lambda}}_n\lambda_n}^H, \end{aligned} \tag{45}$$

where $r_{\lambda_{n'}\lambda_n} = E\{\lambda_{n'}\lambda_n^*\}$ is the statistical correlation between the channels on the n'th and the nth subcarrier, $\mathbf{r}_{\bar{\boldsymbol{\lambda}}_n\lambda_n} = E\{\bar{\boldsymbol{\lambda}}_n\lambda_n^*\}$ is the cross-correlation vector between the channel of interest and the other channels, and $\mathbf{R}_{\bar{\boldsymbol{\lambda}}_n} = E\{\bar{\boldsymbol{\lambda}}_n\bar{\boldsymbol{\lambda}}_n^H\}$ is the cross-correlation matrix of the other channels. Consequently, by defining the $(N-1)\times 1$ zero-mean Gaussian random vector $\boldsymbol{\pi}_n = \hat{\boldsymbol{\lambda}}_n - \boldsymbol{\eta}_{\hat{\boldsymbol{\lambda}}_n} = [\pi_{1,n}\ \cdots\ \pi_{n-1,n}\ \pi_{n+1,n}\ \cdots\ \pi_{N,n}]^T$, (44) becomes

$$\begin{aligned} t_{\mathrm{SC},n,k} &= \lambda_n\left(|\alpha|\rho m s_{n,k} + z_{\mathrm{ICI},n,k} + z_{\mathrm{MAI},n,k} + z_{\mathrm{MAICI},n,k} + z_{\mathrm{IMD},n,k}\right) \\ &\quad + \tilde{z}_{\mathrm{ICI},n,k} + \tilde{z}_{\mathrm{MAICI},n,k} + \tilde{z}_{\mathrm{IMD},n,k} + z_{\mathrm{AWGN},n,k}, \end{aligned} \tag{46}$$

where

$$z_{\mathrm{ICI},n,k} = |\alpha|\rho r_{\lambda_n\lambda_n}^{-1}\sum_{\substack{n'=1\\n'\neq n}}^{N} m_{n,n'}r_{\lambda_{n'}\lambda_n}s_{n',k}, \tag{47}$$

$$z_{\mathrm{MAI},n,k} = |\alpha|m\sum_{\substack{k'=1\\k'\neq k}}^{K}\rho_{k,k'}s_{n,k'}, \tag{48}$$

$$z_{\mathrm{MAICI},n,k} = |\alpha|r_{\lambda_n\lambda_n}^{-1}\sum_{\substack{n'=1\\n'\neq n}}^{N} m_{n,n'}r_{\lambda_{n'}\lambda_n}\sum_{\substack{k'=1\\k'\neq k}}^{K}\rho_{k,k'}s_{n',k'}, \tag{49}$$

$$z_{\mathrm{IMD},n,k} = e^{-j\arg(\alpha)}r_{\lambda_n\lambda_n}^{-1}\sum_{g=0}^{G-1}\theta_{g+1}c_{k,g}^*\sum_{n'=1}^{N} m_{n,n'}r_{\lambda_{n'}\lambda_n}\nu_{\mathrm{IMD},n',g}, \tag{50}$$

$$\tilde{z}_{\mathrm{ICI},n,k} = |\alpha|\rho\sum_{\substack{n'=1\\n'\neq n}}^{N} m_{n,n'}\pi_{n',n}s_{n',k}, \tag{51}$$

$$\tilde{z}_{\mathrm{MAICI},n,k} = |\alpha|\sum_{\substack{n'=1\\n'\neq n}}^{N} m_{n,n'}\pi_{n',n}\sum_{\substack{k'=1\\k'\neq k}}^{K}\rho_{k,k'}s_{n',k'}, \tag{52}$$

$$\tilde{z}_{\mathrm{IMD},n,k} = e^{-j\arg(\alpha)}\sum_{g=0}^{G-1}\theta_{g+1}c_{k,g}^*\sum_{\substack{n'=1\\n'\neq n}}^{N} m_{n,n'}\pi_{n',n}\nu_{\mathrm{IMD},n',g}. \tag{53}$$

We want to highlight by (46) that in the frequency-selective case the ICI consists of two different components. The first one, $\lambda_n z_{\mathrm{ICI},n,k}$, is proportional to the channel amplitude λ_n of the useful signal, and therefore it represents the ICI that fades *coherently* with the useful signal. On the other hand, the second part $\tilde{z}_{\mathrm{ICI},n,k}$ represents the ICI that fades *independently* of λ_n. Indeed, $\tilde{z}_{\mathrm{ICI},n,k}$ in (51) is a zero-mean random variable with power expressed by

$$\tilde{\sigma}_{\mathrm{ICI},n,k}^2 = |\alpha\rho|^2\sum_{\substack{n'=1\\n'\neq n}}^{N}|m_{n,n'}|^2\left(r_{\lambda_{n'}\lambda_n} - r_{\lambda_n\lambda_n}^{-1}|r_{\lambda_{n'}\lambda_n}|^2\right)\sigma_{\mathrm{S}}^2, \tag{54}$$

which does not depend on the actual channel gain λ_n.

Also the MAICI and the IMD, similarly to the ICI, consist of two parts. In both cases, the first part is proportional to λ_n, while the second one has power independent of λ_n. The powers of the second components are expressed, respectively, by

$$\tilde{\sigma}^2_{\mathrm{MAICI},n,k} = |\alpha|^2 \sum_{\substack{n'=1\\ n'\neq n}}^{N} |m_{n,n'}|^2 \left(r_{\lambda_{n'}\lambda_n} - r^{-1}_{\lambda_n\lambda_n} |r_{\lambda_{n'}\lambda_n}|^2\right) \times \sum_{\substack{k'=1\\ k'\neq k}}^{K} |\rho_{k,k'}|^2 \sigma^2_{\mathrm{S}}, \tag{55}$$

$$\tilde{\sigma}^2_{\mathrm{IMD},n,k} = \sum_{g=0}^{G-1}\sum_{g'=0}^{G-1} \theta_{g+1}\theta^*_{g'+1} c^*_{k,g} c_{k,g'} \times \sum_{\substack{n'=1\\ n'\neq n}}^{N}\sum_{\substack{n''=1\\ n''\neq n}}^{N} m_{n,n'} m^*_{n,n''} \left[\mathbf{J}_n^T \mathbf{R}_{\hat{\boldsymbol{\lambda}}_n} \mathbf{J}_n\right]_{n',n''} \times \left[\mathbf{R}_{\mathbf{v}}(g,g')\right]_{n',n''}, \tag{56}$$

where $\mathbf{R}_{\mathbf{v}}(g,g')$ is the same as in (33), and the $(N-1)\times N$ matrix $\mathbf{J}_n$ is obtained from the identity matrix $\mathbf{I}_N$ by removing the nth row. The conditional SINR can be expressed as

$$\gamma_{n,k}(\lambda_n) = \frac{|\lambda_n|^2 |\alpha\rho m|^2 \sigma^2_{\mathrm{S}}}{|\lambda_n|^2 (\sigma^2_{\mathrm{ICI},n,k} + \sigma^2_{\mathrm{MAI},n,k} + \sigma^2_{\mathrm{MAICI},n,k} + \sigma^2_{\mathrm{IMD},n,k}) + \tilde{\sigma}^2_{\mathrm{ICI},n,k} + \tilde{\sigma}^2_{\mathrm{MAICI},n,k} + \tilde{\sigma}^2_{\mathrm{IMD},n,k} + \sigma^2_{\mathrm{AWGN}}}, \tag{57}$$

where

$$\sigma^2_{\mathrm{ICI},n,k} = |\alpha\rho r^{-1}_{\lambda_n\lambda_n}|^2 \sum_{\substack{n'=1\\ n'\neq n}}^{N} |m_{n,n'} r_{\lambda_{n'}\lambda_n}|^2 \sigma^2_{\mathrm{S}}, \tag{58}$$

$$\sigma^2_{\mathrm{MAICI},n,k} = |\alpha r^{-1}_{\lambda_n\lambda_n}|^2 \sum_{\substack{n'=1\\ n'\neq n}}^{N} |m_{n,n'} r_{\lambda_{n'}\lambda_n}|^2 \sum_{\substack{k'=1\\ k'\neq k}}^{K} |\rho_{k,k'}|^2 \sigma^2_{\mathrm{S}}, \tag{59}$$

$$\sigma^2_{\mathrm{IMD},n,k} = r^{-2}_{\lambda_n\lambda_n} \sum_{g=0}^{G-1}\sum_{g'=0}^{G-1} \theta_{g+1}\theta^*_{g'+1} c^*_{k,g} c_{k,g'} \bar{\mathbf{m}}_n^T \mathbf{R}_{\mathbf{v}}(g,g') \bar{\mathbf{m}}_n^*, \qquad \left[\bar{\mathbf{m}}_n\right]_{n'} = m_{n,n'} r_{\lambda_{n'}\lambda_n}, \tag{60}$$

and $\sigma^2_{\mathrm{MAI},n,k}$, $\tilde{\sigma}^2_{\mathrm{ICI},n,k}$, $\tilde{\sigma}^2_{\mathrm{MAICI},n,k}$, and $\tilde{\sigma}^2_{\mathrm{IMD},n,k}$ are expressed by (30), (54), (55), and (56), respectively. Moreover, as in the previous section, we exploit the hypotheses of a high number of subcarriers and a high number of users in order to approximate as Gaussian the interference terms in (46), by the central limit theorem.

The resultant BER can therefore be obtained by inserting (57), (36), and the Rayleigh pdf of $|\lambda_n|$ in (39). Also in this case the BER can be calculated by means of series expansions that involve generalized hypergeometric functions. For 4-QAM, the BER expression is the same as in (37), with

$$\mu^2_{n,k} = \frac{|\alpha\rho m|^2 \sigma^2_{\mathrm{S}} \sigma^2_{\lambda}}{\tilde{\sigma}^2_{\mathrm{ICI},n,k} + \tilde{\sigma}^2_{\mathrm{MAICI},n,k} + \tilde{\sigma}^2_{\mathrm{IMD},n,k} + \sigma^2_{\mathrm{AWGN}}},$$

$$\nu^2_{n,k} = \frac{(\sigma^2_{\mathrm{ICI},n,k} + \sigma^2_{\mathrm{MAI},n,k} + \sigma^2_{\mathrm{MAICI},n,k} + \sigma^2_{\mathrm{IMD},n,k})\sigma^2_{\lambda}}{\tilde{\sigma}^2_{\mathrm{ICI},n,k} + \tilde{\sigma}^2_{\mathrm{MAICI},n,k} + \tilde{\sigma}^2_{\mathrm{IMD},n,k} + \sigma^2_{\mathrm{AWGN}}}. \tag{61}$$

5. SIMULATION RESULTS

In this section, we present some simulation results in order to validate the approximations introduced in the theoretical analysis. We consider an MC-DS-CDMA system with $N = 256$ subcarriers, with a subcarrier separation of $\Delta_f = 1/T = 156.25$ kHz and a cyclic prefix of length $L = 64$. For brevity, we only consider data modulated by 4-QAM, which correspond to a gross bit rate of 4 Mbps per user when the length of the spreading codes is equal to $G = 16$. We assume that each time-domain tap of the channel suffers independent Rayleigh fading, with an exponentially decaying power delay profile and an rms delay spread equal to 250 nanaoseconds.

In the first scenario, we assume that the base station employs Walsh-Hadamard (WH) spreading codes of length $G = 16$. We also assume Hypothesis H1 to be true. We still remark that the BER performance in this scenario can be considered a lower bound for the case of inaccurate estimate of the CFO-induced time-varying phase shift. Figures 1 and 2 show the BER performance versus the received E_b/N_0 when the number of active users is equal to $K = G = 16$. The received E_b/N_0 is defined before the despreading as the ratio between the noiseless signal power and the noise power, while the BER is obtained by averaging the BER over all the subcarriers and all the users. Figure 1 shows the BER versus E_b/N_0 for different values of the normalized CFO ε, assuming linear amplification at the transmitter (i.e., without IMD). The good agreement between theoretical analysis and simulated BER for all practical values of ε is evident. This fact clearly testifies that the Gaussian approximation of the ICI leads to accurate results in frequency-selective scenarios.

Figure 2 illustrates the impact of the NLA on the BER performance in the absence of CFO. We define the output backoff (OBO) as OBO $= P_{\mathrm{U,MAX}}/\sigma^2_{\mathrm{U}}$, where $P_{\mathrm{U,MAX}}$ and σ^2_{U} are the maximum power and the mean power, respectively, of the NLA output signal. We assume that the amplifier

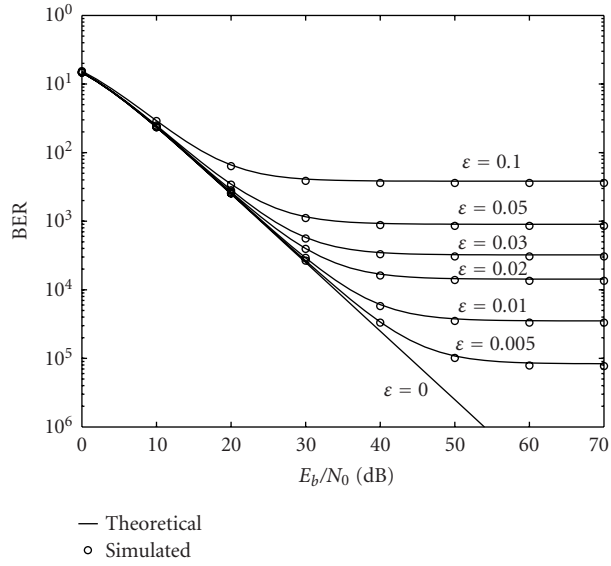

FIGURE 1: Impact of the CFO ε on the BER (WH codes, $K = G = 16$, no IMD).

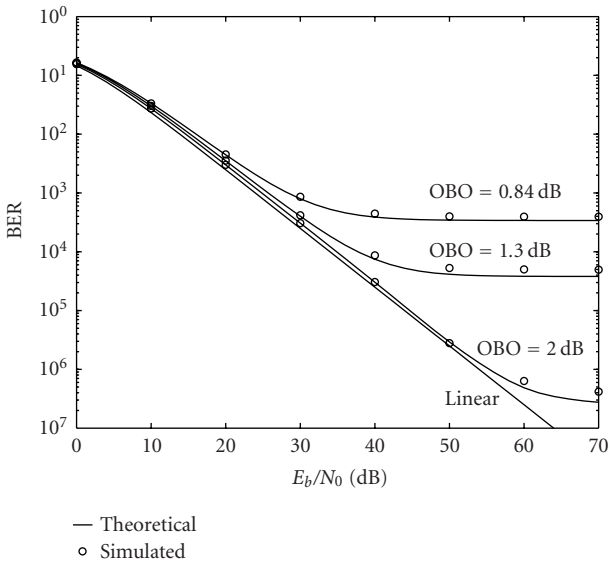

FIGURE 2: Impact of the clipping NLA on the BER (WH codes, $K = G = 16$, no CFO).

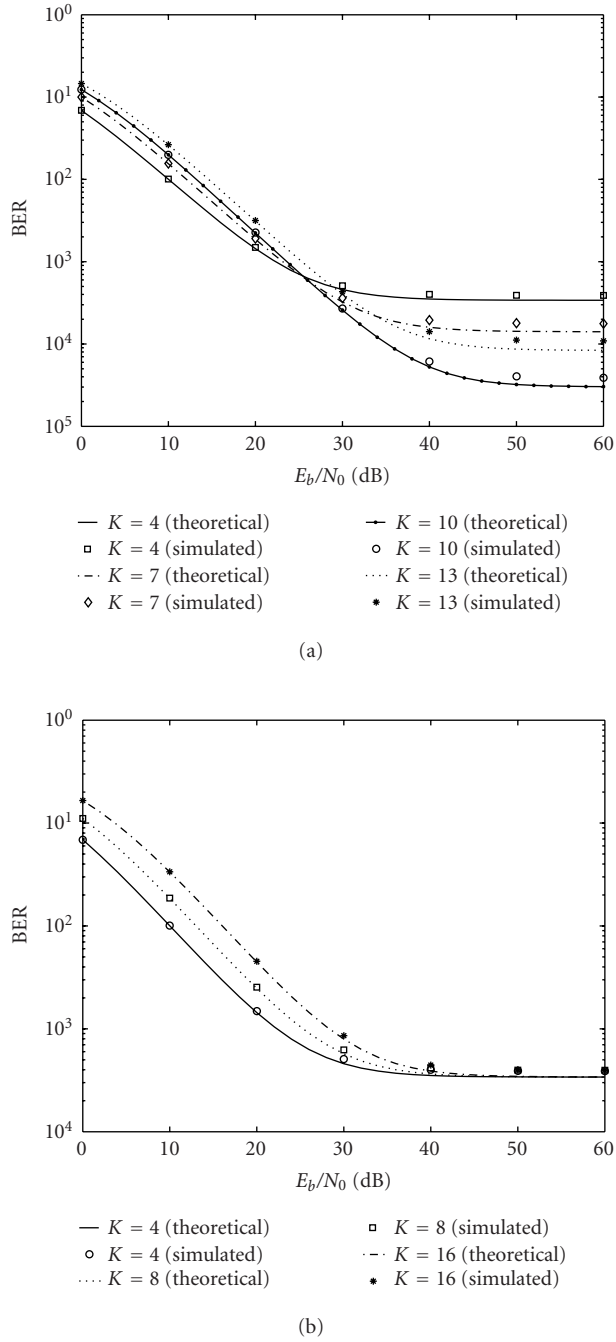

FIGURE 3: BER curves for different number of users K (WH codes, $G = 16$, OBO = 0.84 dB, no CFO).

is perfectly predistorted, that is, it behaves as a clipper of the NLA input envelope. From Figure 2, we deduce that the Gaussian approximation of the IMD is slightly worse than the approximation of the ICI in Figure 1, especially at the saturating BER. Indeed, for a clipping amplifier, the Gaussian approximation of the IMD is very accurate only when the SNR is not too high or the number of subcarriers is very high [24]. However, in this case the BER mismatch seems to be quite small.

In Figures 3a and 3b, we still assume WH spreading codes of length $G = 16$, Hypothesis H1 as true, and $\varepsilon = 0$, and we focus on the impact of the number K of active users on the BER performance. We also assume that each user employs a fixed spreading code, that is, that the kth user employs the kth row of the $G \times G$ Hadamard matrix. Figure 3a shows that at low SNR the BER increases with the number of active users, as expected. However, the BER floor at high SNR does not increase with the number of users.

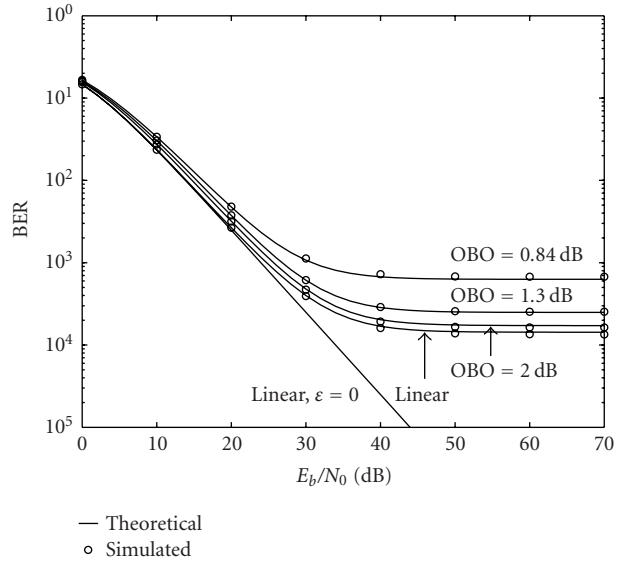

Figure 4: Impact of both CFO and NLA on the BER (WH codes, $K = G = 16$, $\varepsilon = 0.02$).

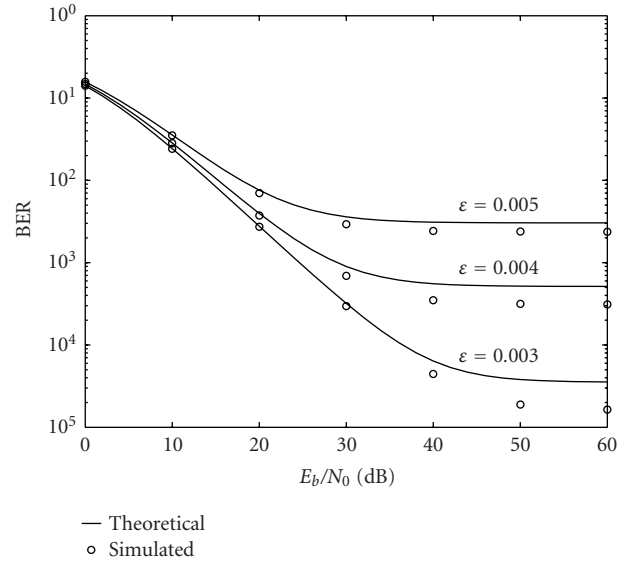

Figure 6: BER curves for different CFO values (Gold codes, $G = 31$, $K = 25$, no IMD).

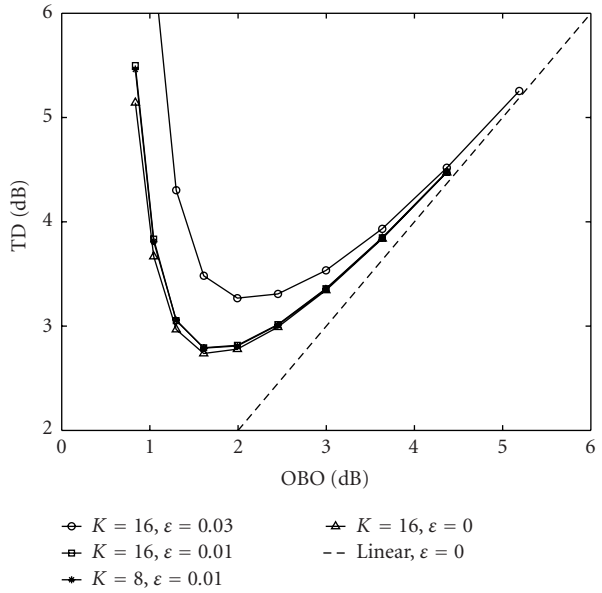

Figure 5: TD as a function of the OBO (WH codes, $G = 16$, BER = 10^{-3}).

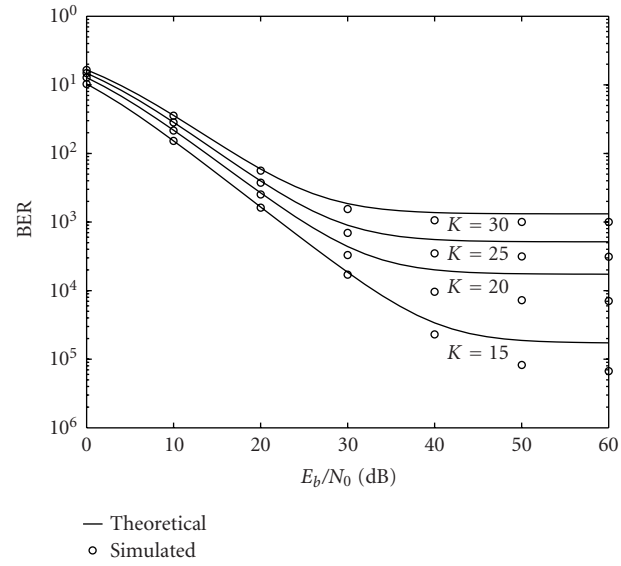

Figure 7: BER curves for different number of users K (Gold codes, $G = 31$, $\varepsilon = 0.004$, no IMD).

Such a behavior is due to the fact that the IMD powers in (56) and (60) depend on $\mathbf{R}_{\mathbf{v}}(g, g')$, which is highly sensitive to the choice of the spreading codes among the ones provided by the Hadamard matrix. This fact is confirmed by the BER floors of Figure 3b, because $\mathbf{R}_{\mathbf{v}}(g, g')$ is the same for $K = 4$, $K = 8$, and $K = 16$.

Figure 4 exhibits the joint effect of CFO and NLA on the BER performance when $\varepsilon = 0.02$. The results show that, in the presence of a CFO, it is not convenient to increase the output NLA power backoff at the transmitter beyond a certain value (that obviously depends on ε), because the IMD reduction is masked by the presence of the ICI induced by the CFO.

In order to identify the optimum OBO value, we introduce the total degradation (TD) as [7]

$$\mathrm{TD}\big|_{\mathrm{dB}} = \Delta_{E_b/N_0}\big|_{\mathrm{dB}} + \mathrm{OBO}\big|_{\mathrm{dB}}, \tag{62}$$

where $\Delta_{E_b/N_0}|_{\mathrm{dB}} = E_b/N_0(\mathrm{OBO}, \varepsilon)|_{\mathrm{dB}} - E_b/N_0(+\infty, \varepsilon)|_{\mathrm{dB}}$ is the SNR increase caused by the NLA to achieve a target BER for a fixed CFO ε. If we neglect out-of-band effects, the minimization of the TD can be considered a fair criterion for

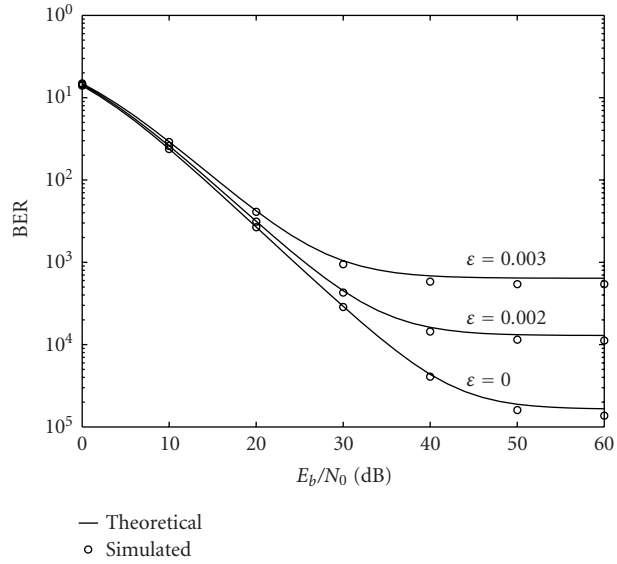

FIGURE 8: BER curves for different CFO values (Gold codes, $G = 31$, $K = 25$, OBO = 2.00 dB).

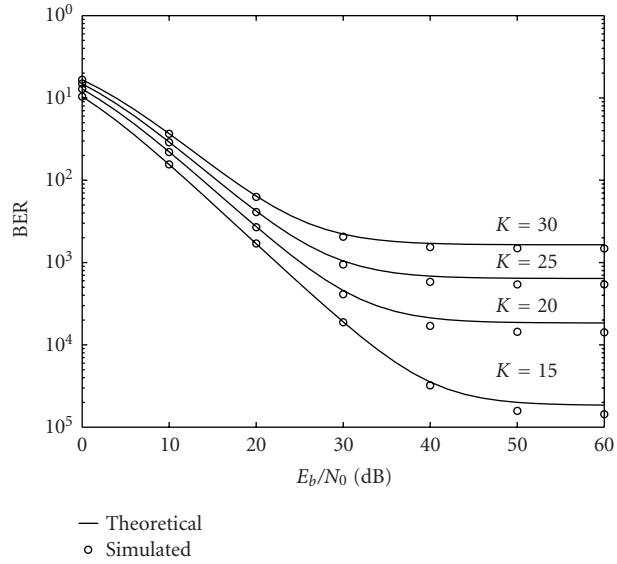

FIGURE 9: BER curves for different number of users K (Gold codes, $G = 31$, $\varepsilon = 0.003$, OBO = 2.00 dB).

the selection of the optimum OBO value, because Δ_{E_b/N_0} and OBO represent the power penalty on the link budget with respect to the linear scenario, and with respect to the maximum amplifier output power, respectively. Figure 5 shows the TD performance at BER $= 10^{-3}$ for different values of the CFO and number of users. It is evident that the optimum OBO mainly depends on the value of the CFO.

In the second simulation scenario, we assume that a rough estimate of the CFO-induced time-varying phase shift is available at the receiver (i.e., Hypothesis H2 is true). In this case, since the MAI cannot be completely eliminated, we assume that the base station employs Gold codes of length $G = 31$. Figures 6 and 7 display the BER performance for different values of the CFO ε and of the number of users K. It is evident that the BER analysis is quite accurate for $E_b/N_0 < 30$ dB, while a certain mismatch between theoretical and simulated BER exists at high SNR. This fact is due to the nonperfect Gaussian approximation of the MAI terms, as confirmed by the estimation of the kurtosis of the decision variable, which is a standard test for non-Gaussian noise [25]. However, the BER mismatch is smaller when also the NLA-induced distortions are present, as testified by Figures 8 and 9 (OBO = 2.00 dB). Figures 6 and 8 clearly show that, if only a rough phase estimate is available, the maximum tolerable CFO is rather small (e.g., $\varepsilon < 0.005$), because of the additional MAI. Therefore, the phase compensation step plays a crucial role in the BER performance of MC-DS-CDMA systems.

6. CONCLUSIONS

In this paper, we have evaluated the BER of MC-DS-CDMA downlink systems subject to both CFO and IMD in frequency-selective Rayleigh fading channels. The BER analysis, which is quite accurate in many conditions, allows to identify the optimum OBO value of the NLA, depending on the amount of CFO. The analytical findings have also highlighted the importance of an accurate compensation for the CFO-induced phase shift. Although the analysis has been carried out for M-ary QAM, it can also be extended to M-ary phase-shift keying constellations. Future works may focus on the effects of channel estimation errors and channel coding.

ACKNOWLEDGMENTS

The authors would like to thank Prof. Geert Leus for his insightful comments and suggestions. This work was partially supported by the Italian Ministry of Education, University and Research, PRIN 2002 Project "MC-CDMA: an air interface for the 4th generation of wireless systems."

REFERENCES

[1] S. Hara and R. Prasad, "Overview of multicarrier CDMA," *IEEE Commun. Mag.*, vol. 35, no. 12, pp. 126–133, 1997.

[2] K. Fazel and G. P. Fettweis, Eds., *Multi-Carrier Spread-Spectrum*, Kluwer Academic Publishers, Dordrecht, Netherlands, 1997.

[3] T. Pollet, M. Van Bladel, and M. Moeneclaey, "BER sensitivity of OFDM systems to carrier frequency offset and Wiener phase noise," *IEEE Trans. Commun.*, vol. 43, no. 2/3/4, pp. 191–193, 1995.

[4] H. Ochiai and H. Imai, "On the distribution of the peak-to-average power ratio in OFDM signals," *IEEE Trans. Commun.*, vol. 49, no. 2, pp. 282–289, 2001.

[5] S. Verdú, *Multiuser Detection*, Cambridge University Press, Cambridge, UK, 1998.

[6] H. Steendam and M. Moeneclaey, "The sensitivity of downlink MC-DS-CDMA to carrier frequency offsets," *IEEE Commun. Lett.*, vol. 5, no. 5, pp. 215–217, 2001.

[7] J.-H. Jong and W. E. Stark, "Performance analysis of coded multicarrier spread-spectrum systems in the presence of multipath fading and nonlinearities," *IEEE Trans. Commun.*, vol. 49, no. 1, pp. 168–179, 2001.

[8] Z. Wang and G. B. Giannakis, "Wireless multicarrier communications," *IEEE Signal Processing Mag.*, vol. 17, no. 3, pp. 29–48, 2000.

[9] A. Papoulis, *Probability, Random Variables and Stochastic Processes*, McGraw-Hill, New York, NY, USA, 3rd edition, 1991.

[10] P. Banelli and S. Cacopardi, "Theoretical analysis and performance of OFDM signals in nonlinear AWGN channels," *IEEE Trans. Commun.*, vol. 48, no. 3, pp. 430–441, 2000.

[11] D. Dardari, V. Tralli, and A. Vaccari, "A theoretical characterization of nonlinear distortion effects in OFDM systems," *IEEE Trans. Commun.*, vol. 48, no. 10, pp. 1755–1764, 2000.

[12] X. Ma, C. Tepedelenlioğlu, G. B. Giannakis, and S. Barbarossa, "Non-data-aided carrier offset estimators for OFDM with null subcarriers: identifiability, algorithms, and performance," *IEEE J. Select. Areas Commun.*, vol. 19, no. 12, pp. 2504–2515, 2001.

[13] T. M. Schmidl and D. C. Cox, "Robust frequency and timing synchronization for OFDM," *IEEE Trans. Commun.*, vol. 45, no. 12, pp. 1613–1621, 1997.

[14] H. Minn, M. Zeng, and V. K. Bhargava, "On timing offset estimation for OFDM systems," *IEEE Commun. Lett.*, vol. 4, no. 7, pp. 242–244, 2000.

[15] D. Landström, S. K. Wilson, J.-J. van de Beek, P. Ödling, and P. O. Börjesson, "Symbol time offset estimation in coherent OFDM systems," *IEEE Trans. Commun.*, vol. 50, no. 4, pp. 545–549, 2002.

[16] K.-W. Yip and T.-S. Ng, "Effects of carrier frequency accuracy on quasi-synchronous, multicarrier DS-CDMA communications using optimized sequences," *IEEE J. Select. Areas Commun.*, vol. 17, no. 11, pp. 1915–1923, 1999.

[17] P. H. Moose, "A technique for orthogonal frequency division multiplexing frequency offset correction," *IEEE Trans. Commun.*, vol. 42, no. 10, pp. 2908–2914, 1994.

[18] R. Van Nee and R. Prasad, *OFDM for Wireless Multimedia Communications*, Artech House, Boston, Mass, USA, 2000.

[19] K. Cho and D. Yoon, "On the general BER expression of one- and two-dimensional amplitude modulations," *IEEE Trans. Commun.*, vol. 50, no. 7, pp. 1074–1080, 2002.

[20] L. Rugini, P. Banelli, and S. Cacopardi, "An analytical upper bound on MMSE performance using approximated MMSE multiuser detector in flat Rayleigh fading channels," in *Proc. European Wireless Conference*, pp. 952–956, Florence, Italy, February 2002.

[21] L. Rugini and P. Banelli, "Symbol error probability of linearly modulated signals affected by Gaussian interference in Rayleigh fading channels," Tech. Rep. RT-005-03, Department of Electronic and Information Engineering, University of Perugia, Perugia, Italy, December 2003, http://www.diei.unipg.it/rt/DIEI_RT.htm.

[22] I. S. Gradshteyn and I. M. Ryzhik, *Table of Integrals, Series, and Products*, Academic Press, San Diego, Calif, USA, 5th edition, 1994.

[23] S. M. Kay, *Fundamentals of Statistical Signal Processing: Estimation Theory*, vol. 1, Prentice Hall, Englewood Cliffs, NJ, USA, 1993.

[24] H. Nikopour and S. H. Jamali, "Effects of Cartesian clipping noise on the performance of orthogonal frequency division multiplexing system: a theoretical approach," in *Proc. IEEE Global Telecommunications Conference (GLOBECOM '02)*, vol. 2, pp. 1254–1258, Taipei, Taiwan, November 2002.

[25] S. M. Kay, *Fundamentals of Statistical Signal Processing: Detection Theory*, vol. 2, Prentice Hall, Englewood Cliffs, NJ, USA, 1998.

Luca Rugini was born in Perugia, Italy, in 1975. He received the Laurea degree in electronics engineering and the Ph.D. degree in telecommunications from the University of Perugia, Perugia, Italy, in 2000 and 2003, respectively. He is currently a postdoctoral researcher with the Department of Electronic and Information Engineering (DIEI), the University of Perugia. His research interests include spread-spectrum and multicarrier communications.

Paolo Banelli was born in Perugia, Italy, on May 19, 1968. He received the Laurea degree in electronics engineering and the Ph.D. degree in telecommunications from the University of Perugia, Perugia, Italy, in 1993 and 1998, respectively. Since 1998, he has been an Assistant Professor with the Department of Electronic and Information Engineering (DIEI), University of Perugia. In 2001, he joined as a Visiting Researcher the Spin-Comm Group at the Electrical and Computer Engineering (ECE) Department, University of Minnesota, Minneapolis. His research interests include nonlinear distortions, broadcasting, multiuser detection, multicarrier, and block-transmission techniques for wireless communications.